Journal of Magnetism and Magnetic Materials 430 (2017) 65–69

Contents lists available at ScienceDirect

Journal of Magnetism and Magnetic Materials

journal homepage: www.elsevier.com/locate/jmmm

First principles electronic structure and magnetic properties of inverse Heusler alloys X_2YZ(X=Cr; Y=Co, Ni; Z=Al, Ga, In, Si, Ge, Sn, Sb)

Susanta K. Mohanta[a,b], Yongxue Tao[a], Xiaoyan Yan[a], Guanhua Qin[a], Venkatesh Chandragiri[a,b], Xi Li[c], Chao Jing[a], Shixun Cao[a,b], Jincang Zhang[a,b], Zhenhua Qiao[d], Hui Gu[b], Wei Ren[a,b,*]

[a] Department of Physics, and International Centre for Quantum and Molecular Structures, Shanghai University, Shanghai 200444, China
[b] Materials Genome Institute, and Shanghai Key Laboratory of High Temperature Superconductors, Shanghai University, Shanghai 200444, China
[c] State Key Laboratory of Advanced Special Steel, Shanghai University, Shanghai 200072, China
[d] ICQD, Hefei National Laboratory for Physical Sciences at Microscale, Synergetic Innovation Centre of Quantum Information and Quantum Physics, CAS Key Laboratory of Strongly-Coupled Quantum Matter Physics and Department of Physics, University of Science and Technology of China, Hefei, Anhui 230026, China

ABSTRACT

Using augmented plane wave+local orbital basis, we have calculated the electronic structure and magnetic properties of X_2YZ (X=Cr; Y=Co and Ni; Z=Al, Ga, In, Si, Ge, Sn, Sb) inverse Heusler alloys from first principles. We employ the Hg_2CuTi type $L2_1$ structure which indeed provides the low energy solution. The calculated total magnetic moments considered here follow the generalized Slater-Pauling behavior ($Z_t - 24$) except Cr_2NiSb, which shows ($Z_t - 28$) instead. These materials show a systematic trend of ferrimagnetic Cr-Cr exchange interaction which increases with the number of valence electrons. The half-metallic and ferrimagnetic behaviors make them promising candidates for spintronic materials and devices.

1. Introduction

Since the prediction of half-metallic ferromagnetism in NiMnSb by de Groot et al. [1], half Heusler and Heusler compounds have received enormous interest because of their potential applications in spintronic devices [2–4]. The Heusler compounds exhibit diverse magnetic phenomena and have been in the forefront of research activity from last two decades [5,6]. In few cases, at Fermi energy (E_F) one spin direction is metallic and the other has a semiconducting gap, demonstrating 100% spin polarization, and maximizing the efficiency of spintronic devices [7–9]. Thus in principle they can be used for perfect spin filters [10], spin injection devices [11] or magnetoresistive devices [12] with infinite magnetoresistance. Apart from these, there has been lot of excitement regarding the magnetocaloric and theromoelectric effects of Heusler compounds [13–15]. Experimentally it has been observed that *M*NiSn-based half-Heusler systems, where *M*=Ti, Hf, Zr, exhibit excellent *n*-type theromoelectric properties with large power factor and figure of merit 0.8 at 1000 K [16]. For the *p* type, on the other hand, *M*CoSb compounds (M=Ti, Hf, Zr), appear to be promising at high temperature and have been extensively studied experimentally [17–22]. Although a large number of half-metallic Heusler compounds have been studied, novel properties are still to be discovered, e.g., ferromagnetic or ferrimagnetic semiconducting behavior, to pave the way for diverse applications in spintronics/magnetoelectronics [23–26].

On the theoretical side, there have been several reports of electronic structure and magnetic properties of full and half-Heusler compounds. The family of Heusler compounds incorporate more than 1000 members almost all crystallizing in close-packed cubic structure similar to the binary semiconductors [27]. The crystal structure of ternary Heusler alloys can be broadly classified into two classes, the half (or semi-) Heusler alloys have the chemical formula XYZ and full Heusler compounds are X_2YZ. The X and Y are transition-metal elements and Z is an *sp*-element. In the case of full-Heusler compounds, when the valence of X is larger than Y, the atomic sequence is X-Y-X-Z along the diagonal direction of cubic cell and the structure is well known $L2_1$. When the valency of the Y element is largest, the compounds crystallize in the so-called *XA* structure, in which the sequence of atoms is X-X-Y-Z and commonly known as inverse-Heusler alloys (see Fig. 1) [28]. Several recent first-principles electronic structure calculations confirm that indeed the X-X-Y-Z sequence with prototype of Hg_2CuTi [29] is energetically favorable [30–35]. Experimentally the inverse Heusler structure was also confirmed in Mn_2CoGa and Mn_2CoSn thin films as well as Co doped Mn_3Ga samples [36–39]. Inverse Heuslers combine

* Corresponding author at: Department of Physics, and International Centre for Quantum and Molecular Structures, Shanghai University, Shanghai 200444, China.
E-mail address: renwei@shu.edu.cn (W. Ren).

http://dx.doi.org/10.1016/j.jmmm.2017.01.055
Received 28 November 2016; Received in revised form 9 January 2017; Accepted 16 January 2017
Available online 22 January 2017
0304-8853/

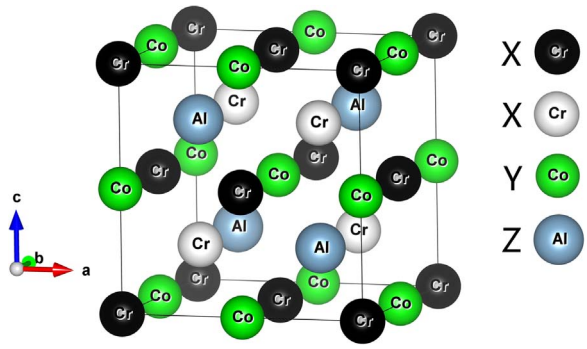

Fig. 1. Schematic representation of Hg_2CuTi-type XA structure. The lattice consists of four face-centred cubic (fcc) sublattices. The unit cell is that of fcc lattice with four atoms as basis: X at (0 0 0) and (1/4 1/4 1/4), Y at (1/2 1/2 1/2) and Z at (3/4 3/4 3/4). X=Cr; Y=Co and Ni; Z=Al, Ga, In, Si, Ge, Sn, Sb.

coherent growth on semiconductors with Curie temperature exceeding 1000 K in the case of Cr_2CoGa and are interesting candidates for practical applications [25]. Skaftouros et al., have done a series of calculations on many inverse Heusler alloys explaining the generalized Slater-Pauling behavior [28]. In this paper, we present new results of self-consistent first-principles calculations of inverse Heusler alloys X_2YZ(X=Cr; Y=Co, Ni; Z=Al, Ga, In, Si, Ge, Sn, Sb), which show the effect of *p* electrons on the ferrimagnetic coupling of Cr-Cr atoms and generalized Slater-Pauling behavior.

2. Computational details

The calculations presented in this paper have been performed within the framework of density functional theory [40–42], using the augmented plane wave+local orbital (APW+lo) method [42–44] as implemented in the WIEN2k package [45]. In the APW+lo method, the unit cell is divided into two parts: i) non-overlapping muffin-tin sphere of radius R_{MT} and ii) the remaining interstitial region. For our calculations, we have used R_{MT}=2.25–2.35 a.u. for transition metal atoms and R_{MT}=2.1–2.3 a.u. for *p* elements. The wave functions within the atomic spheres are expanded in spherical harmonics with maximum multipolarity l_{max}=10. The wave functions in the interstitial region were expanded as plane waves with a cutoff wave vector $K_{max}=7.5/R_{MT}^{min}=3.57$. The charge density was Fourier expanded up to $G_{max} = 16\sqrt{Ry}$. For exchange and correlation, we have used the Perdew-Burke-Ernzerhof formalism of the generalized gradient approximation (GGA) [46]. For sampling of the Brillouin zone, a k-mesh of size 20 × 20 × 20 with 256 special k points in the irreducible wedge of the Brillouin zone was used. For all calculations lattice relaxation was applied to minimize the force on the atoms to less than 1 mRy/a.u. The self consistency of the calculations was ascertained from the charge and energy convergence criterion set to be 0.0001 and 0.01 mRy respectively. The results of Wien2k are also compared with VASP [47] calculations with projector augmented plane wave method [48]. An energy cutoff of 450 eV was used for the plane wave expansion, with an total energy convergence of the order of 10^{-4} eV and same size of *k*-mesh grid as mentioned before.

3. Results and discussion

The full-Heusler compounds discussed here are crystallized in the Hg_2CuTi-type XA structure, the typical sequence of the chemicals are X-X-Y-Z along the diagonal direction of cubic cell. This exchange arrangement of atoms means that two Cr atoms are no longer equivalent. A schematic representation of the inverse Heusler compounds is given in Fig. 1. There are four atoms along the diagonal of the cube following the above mentioned sequence. It is clear that the two X atoms sit at sites of different symmetry. We have used black and white

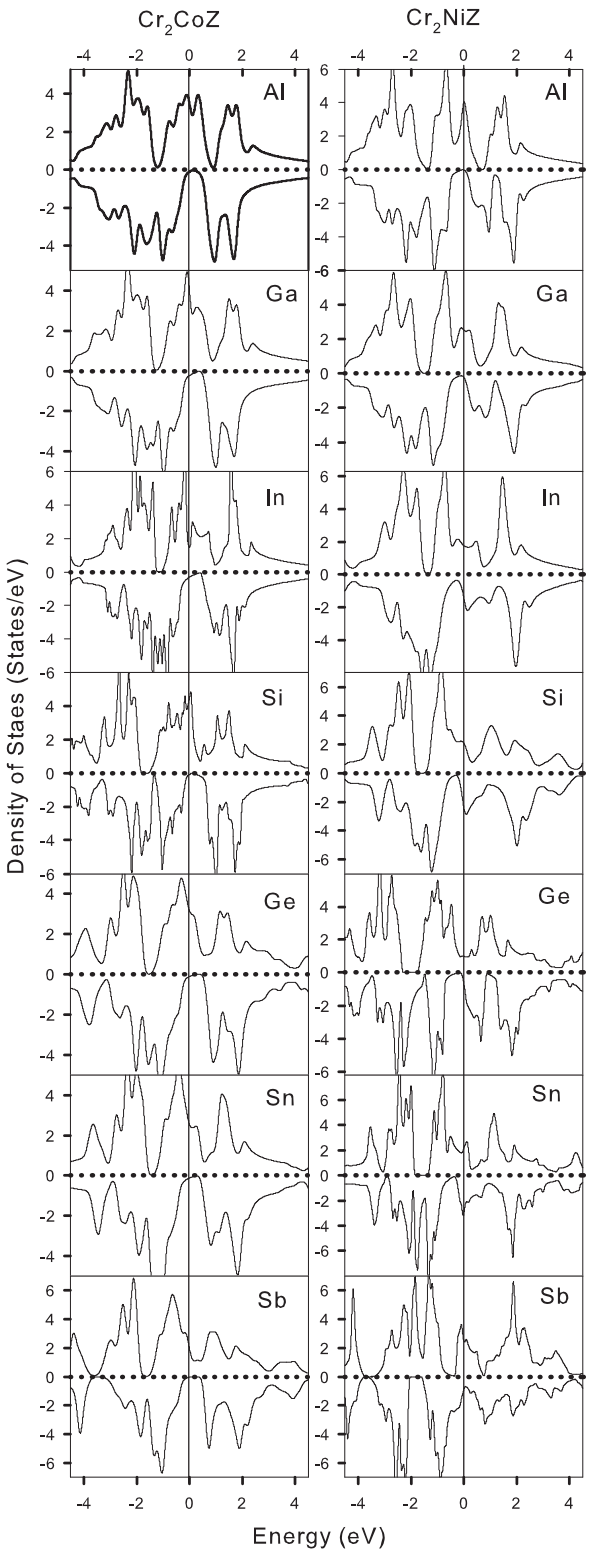

Fig. 2. Total density of states for the Cr_2CoZ (left panel) and the Cr_2NiZ (right panel), Z=Al, Ga, In, Si, Ge, Sn, Sb. The solid vertical line represents the Fermi level.

colors to distinguish between them. One of the Cr (black) atoms is surrounded by four nearest-neighboring Cr atoms (white) and four Z type atoms, whereas the other Cr (white) is surrounded by four Cr (black) and four Y-type atoms. Concerning the next-nearest neighbors, X (black) site has six Y atoms as second neighbors, and Y site has six X (black) atoms as second neighbors. The equivalent is the situation for X (white) and Z atomic sites. Here we would like to mention that the

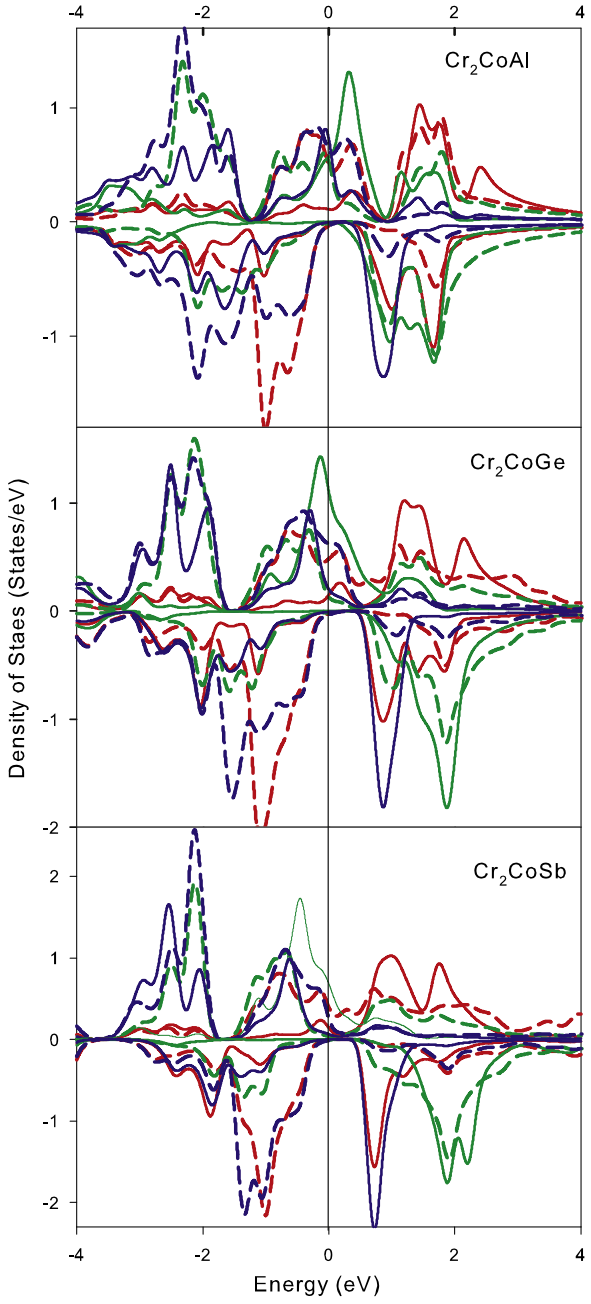

Fig. 3. Spin projected d electrons DOS of both Cr and Y atoms for three representative cases (Cr_2CoZ (Z=Al, Ga, Sb)). Solid lines are for e_g and dashed lines represent t_{2g} states. Red: Cr(A); Green: Cr(B) and Blue: Co (Y). (For interpretation of the references to color in this figure legend, the reader is referred to the web version of this article.)

Hg_2CuTi-type XA structure provides the low energy solution compared to $L2_1$ X-Y-X-Z structure, agreeing with previous studies [49,29].

We show the spin-resolved total density of states (DOS) for both up and down spin in Fig. 2 for all cases calculated here. The vertical line indicates the position of Fermi level (E_F). It is interesting to note that, in the case of Cr_2CoZ (Z=Al, Ga, In, Si, Ge, Sn, Sb) the E_F straddles in the low-energy part of the half-metallic gap whereas, in Cr_2NiX it moves to higher energies. This can be interpreted as due to increase of one *d* band electron the Fermi level moves to higher energies. The band broadening reduces the characteristic half-metallic feature which can be restored by lattice expansion as shown in Ref [50]. The spin-projected partial density of states show very strong hybridization between the *d* orbitals of transition elements and a broad delocalized behavior (see Fig. 3). The extent of delocalization contracts as the lattice expands with the increase in number of electrons. The valence band extends up to 5 eV below the Fermi level and the majority DOS shows a large peak just below the Fermi level like a virtual bound state. The typical gap feature on the minority band is of the order of 0.2–0.4 eV depending on the material, and Fermi level falls within the gap with negligible DOS agreeing with previous calculations [49,51].

Table 1
Calculated lattice parameters in Å and spin magnetic moments in μ_B, the two distinct X atomic sites are labeled as A and B. Z_t represents the total number of valence electrons.

	a (Å)	$m_{[X^A]}$	$m_{[X^B]}$	$m_{[Y]}$	$m_{[Z]}$	$m_{[tot]}$	Z_t
Cr_2CoAl	5.72	−1.40	1.29	0.24	−0.047	0.009	24
Cr_2CoGa	5.73	−1.66	1.48	0.36	−0.036	0.076	24
Cr_2CoIn	5.98	−2.33	2.06	0.58	−0.041	0.130	24
Cr_2CoSi	5.65	−0.84	1.32	0.58	−0.015	1.006	25
Cr_2CoGe	5.79	−1.50	1.95	0.63	−0.023	1.020	25
Cr_2CoSn	5.98	−1.96	2.32	0.74	−0.030	1.030	25
Cr_2CoSb	6.05	−1.53	2.50	1.03	−0.008	2.002	26
Cr_2NiAl	5.83	−1.58	2.11	0.50	−0.027	1.000	25
Cr_2NiGa	5.86	−1.86	2.37	0.49	−0.016	1.009	25
Cr_2NiIn	6.17	−2.57	2.91	0.45	−0.016	0.808	25
Cr_2NiSi	5.70	−2.09	2.95	0.62	0.028	1.605	26
Cr_2NiGe	5.76	−0.94	2.22	0.60	−0.005	1.951	26
Cr_2NiSn	6.17	−2.70	2.90	0.34	−0.056	2.50	26
Cr_2NiSb	6.13	2.002	−2.91	−0.32	−0.015	−1.338	27

The calculated spin magnetic moments are shown in Table 1. As the orbital contributions are negligibly small we have not included spin-orbit coupling [52]. The crystal has tetrahedral symmetry (T_d), where the *d* orbital split into two fold degenerate e_g bands and three fold degenerate t_{2g} bands. For better illustration we have plotted the e_g and t_{2g} states of atoms at X and Y sites for three cases (see Fig. 3). Due to point group symmetry, overlapping between e_g orbitals of two distinct Cr atoms is possible and also the same for t_{2g} states, thereby creating five bonding and five anti-bonding orbitals. The double-degenerate e_g states that lie very low in energy below the Fermi level (E_F) are occupied and the antibonding states those are above E_F are unoccupied. Finally, for the case of Y atoms (e.g. Co and Ni in our cases) the nonbonding t_{1u} states are occupied and the e_u states remain on the antibonding region. Here we would like to mention that, it is difficult to distinguish from t_{2g} to t_{1u} and e_g from e_u, except a broad hump below the Fermi level on the t_{2g} band of Co which do not completely overlap with the Cr t_{2g} as they are in the second nearest-neighbor position (see e.g. Fig. 3, the spin down band of Co in the cases of Cr_2CoGe). The general nomenclature schemes and origin of the Slater-Pauling (SP) behavior have been discussed by Galankis et al., in Ref. [51] (and references therein). A possible hybridization between the D-orbitals is schematically shown in Fig. 4.

The half-metallic property is quite prominent in the cases studied here. The calculated magnetic moments show a systematic trend, when

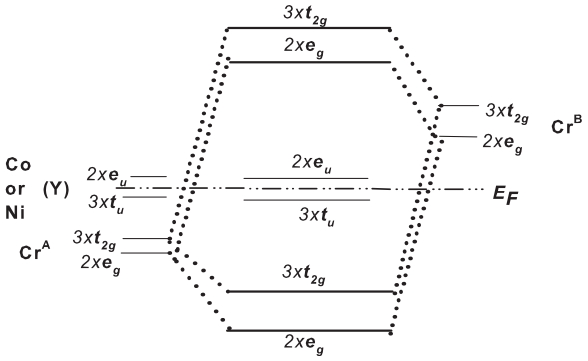

Fig. 4. Possible hybridization between spin-down orbitals sitting at different sites. The names of the orbitals and the superscripts follow the nomenclature discussed in the text. The numbers represents the degeneracy of the orbitals.

we move from group III to group IV at the Z site, thereby populating one more valence p electron on the spin-down state and the total magnetic moment increases by one unit. The two distinct Cr sites couple ferrimagnetically and the ferrimagnetic exchange increases as we move down the group. The Y site (Co or Ni) couples ferromagnetically with the nearest neighbor Cr and antiferromagnetically with second nearest neighbor Cr. The magnetic moments in the unit cell follow the generalized SP ($Z_t - 24$) rule as discussed in detail by Galankis et al. in Ref.[51] except for the Cr_2NiSb which follows $Z_t - 28$ behavior. The magnetic moments of Cr vary from 0.9 μ_B to 3 μ_B and two distinct sites couple ferrimagnetically. Despite strong hybridization, the atom at the Y site also carries moment which increases as the unit cell volume increases (see Fig. 3). This can be understood since the Fermi level shifts to higher energies to accommodate more electrons. We have observed as high as 1 μ_B for Co in the case of Cr_2CoSb. The Z atoms carry negligible spin magnetic moment. The magnetic moment gained at the Z site is possibly induced due to $sp - d$ hybridization. The relative orientation of spin magnetic moments of Y is parallel to nearest neighbor Cr, except for the case of Cr_2NiSb, which tend to have antiparallel spin magnetic moment to their nearest neighbors. Here we would like to mention that the results of our calculations are consistent with some available previous calculations [28], and future experimental results are expected for comparison with our new computational data.

The principal reason for the loss of half-metallic characteristic for the Ni based materials is due to the shift of the bands relative to E_F. A smaller lattice parameter causes broader bands and vice versa. We also note that, in most of the cases the total moment deviates from integer value, a necessary condition for 100% spin polarization. The half-metallic properties can further be enhanced by growing these materials with state-of-the-art techniques like the molecular beam epitaxy or pulsed laser deposition, so that the lattice parameters will be imposed by the substrate and growth conditions like temperature and pressure. So these candidates are promising materials for spin-based applications. Nowadays, antiferromagnetic tips are used in scanning tunneling microscopy (STM) to avoid the stray field induced in case of a ferromagnetic tip. In STM tunneling electrons come from the very same atom most close to the surface. Therefore, as the magnetization of this atom is well defined, the tunneling current remains polarized for antiferromagnetic tips but without stray field. The studied materials Cr_2Co(Al, Ga, In) can be promising materials for STM tip as the Curie temperature is unexpectedly high in Cr_2CoGa [25].

4. Summary

In summary, using the augmented plane wave+local orbital (APW +lo) method based on the density function theory we have carried out ab-initio calculations of Cr based inverse-Heusler alloys. These materials are promising candidates for half-metallic magnetic systems that can be used in spin based electronics and STM tip. We have considered the Hg_2CuTi type XA Structure which is energetically favorable. The Y site (Co or Ni) moment couples parallel with nearest neighbor Cr and antiparallel with the next nearest neighbor Cr. Moreover ferrimagnetism co-exist with half-metallicity, resulting in the fully compensated half-metallic ferrimagnetism in Cr_2CoZ (Z=Al, Ga, In), which may show large exchange bias and lead to the development of magneto-electronic devices. The magnetic moments of the unit cell are found to follow the generalized Slater-Pauling behavior.

Acknowledgement

This work was supported by the National Natural Science Foundation of China (11274222, 51672171 and 51371111), the National Key Basic Research Program of China (2015CB921600), the Eastern Scholar Program from the Shanghai Municipal Education Commission (GZ2015010). Special Program for Applied Research on Super Computation of the NSFC-Guangdong Joint Fund (the second phase), and Shanghai Supercomputer Center are also acknowledged.

References

[1] R.A. de Groot, F.M. Muller, P.G. van Engen, K.H.J. Buschow, Phys. Rev. Lett. 50 (1983) 2024.
[2] S.A. Wolf, D.D. Awschalom, R.A. Buhrman, J.M. Daughton, S. von Molnar, M.L. Roukes, A.Y. Chtchelkanova, D.M. Treger, Science 294 (2001) 1488.
[3] C.M. Fang, G.A. de Wijis, R.A. de Groot, J. Appl. Phys. 91 (2002) 8340.
[4] Y. Jin, P. Kharel, P. Lukashev, S. Valloppilly, B. Staten, J. Herran, I. Tutic, M. Mitrakumar, B. Bhusal, A. OConnell, K. Yang, Y. Huh, R. Skomski, D.J. Sellmyer, J. Appl. Phys. 120 (2016) 053903.
[5] [a] I. Žutic, J. Fabian, S.Das Sarma, Rev. Mod. Phys. 76 (2004) 323;
[b] C. Felser, G.J. Fecher, B. Balke, Angew. Chem. Int. Ed. 46 (2007) 668.
[6] M.I. Katsnelson, V.Yu. Irkhin, L. Chioncel, A.I. Lichtenstein, R.A. de Groot, Rev. Mod. Phys. 80 (2008) 315.
[7] Yurong Yang, Yang. Xiao, Wei Ren, X.H. Yan, Fengming. Pan, Phys. Rev. B 84 (2011) 195447.
[8] M. Bowen, A. Barthélèmy, M. Bibes, E. Jacquet, J.P. JContour, D. Wortmann, S. Blügel, J. Phys. :Condens. Matter 17 (2015) L407.
[9] P. Lukashev, P. Kharel, S. Gilbert, B. Staten, N. Hurley, R. Fuglsby, Y. Huh, S. Valloppilly, W. Zhang, K. Yang, R. Skomski, D.J. Sellmyer, Appl. Phys. Lett. 108 (2016) 141901.
[10] K.A. Killan, R.H. Victora, J. Appl. Phys. 87 (2000) 7064.
[11] S. Datta, B. Das, Appl. Phys. Lett. 56 (1990) 665.
[12] Bin. Wang, Yu. Zhu, Wei. Ren, Jian. Wang, Hong. Guo, Phys. Rev. B 75 (2007) 235415.
[13] S. Sakurada, N. Shutoh, Appl. Phys. Lett. 86 (2005) 082105.
[14] Zhe Li, Kun Xu, Yuanlei Zhang, Chang Tao, Dong Zheng, Chao Jing, Sci. Rep. 5 (2015) 15143.
[15] C. Jing, X.L. Wang, P. Liao, Z. Li, Y.J. Yang, B.J. Kang, D.M. Deng, S.X. Cao, J.C. Zhang, J. Zhu, J. Appl. Phys. 114 (2013) 063907.
[16] S.R. Culp, S.J. Poon, N. Hickmn, T.M. Tritt, J. Blumm, Appl. Phys. Lett. 88 (2006) 042106.
[17] Y. Xia, S. Bhattacharaya, V. Ponnambalam, A.L. Pope, S.J. Poon, T.M. Tritt, J. Appl. Phys. 88 (2000) 1952.
[18] Y. Xia, V. Ponnambalam, S. Bhattacharaya, A.L. Pope, S.J. Poon, T.M. Tritt, J. Phys.: Condens. Matter 13 (2001) 77.
[19] T. Sekimoto, K. Kurosaki, H. Muta, S. Yamanaka, Jpn. J. Appl. Phys. 46 (2007) L673.
[20] S.R. Culp, J.W. Simonson, S.J. Poon, V. Ponnambalam, J. Edwards, T.M. Tritt, Appl. Phys. Lett. 93 (2008) 022105.
[21] W. Xie, Q. Jin, X. Tang, J. Appl. Phys. 106 (2008) 043711.
[22] P. Qiu, X. Huang, X. Chen, L. Chen, J. Appl. Phys. 106 (2009) 103703.
[23] I. Galankis, K. Özdoğan, E. Sasioğlu, Appl. Phys. Lett. 103 (2013) 142404.
[24] I. Galankis, K. Özdoğan, E. Sasioğlu, J. Phys.: Condens. Matter 26 (2014) 086003.
[25] I. Galankis, E. Sasioğlu, Appl. Phys. Lett. 99 (2011) 052509.
[26] Hirohata, K. Takanashi, J. Phys. D: Appl. Phys. 47 (2014) 193001.
[27] T. Graf, C. Felser, S.S.P. Parkin, Prog. Solid State Chem. 39 (2011) 1.
[28] S. Skaftouros, K. Özdogan, E. Sasioğlu, I. Galankis, Phys. Rev. B 87 (2013) 024420.
[29] K. Özdogan, I. Galankis, J. Magn. Magn. Mater. 321 (2009) L34.
[30] G.D. Liu, X.F. Dai, H.Y. Liu, J.L. Chen, Y.X. Li, G. Xiao, G.H. Wu, Phys. Rev. B 77 (2008) 014424.
[31] M. Meinert, J.-M. Schmalhorst, G. Reiss, J. Phys.: Condens. Matter 23 (2011) 116005.
[32] H. Luo, Z. Zhu, L. Ma, S. Xu, X. Zhu, C. Jiang, H. Xu, G. Wu, J. Phys. D 41 (2008) 055010.
[33] J. Li, H. Chen, Y. Li, Y. Xiao, Z. Li, J. Appl. Phys. 105 (2009) 083717.
[34] B. Xu, M. Zhang, H. Yan, Phys. Status Solidi B 248 (2870) (2011).
[35] [a] N. Kervan, S. Kervan, J. Phys. Chem. Solid 72 (2011) 1385;
[b] N. Kervan, S. Kervan, Solid State Commun. 151 (2011) 1162;
[c] N. Kervan, S. Kervan, J. Magn. Magn. Mater. 324 (2012) 645;
[d] E. Bayar, N. Kervan, S. Kervan, Ibid 323 (2011) 2945.
[36] J. Winterlik, G.H. Fecher, B. Balke, T. Graf, V. Alijani, V. Ksenofontov, C.A. Jenkins, O. Meshcheriakova, C. Felser, G. Liu, S. Ueda, K. Kobayashi, T. Nakamura, M. Wojcik, Phys. Rev. B 83 (2011) 174448.
[37] M. Meinert, J.M. Schmalhorst, C. Klewe, G. Reiss, E. Arenholz, T. Bohnert, K. Nielsch, Phys. Rev. B 84 (2011) 132405.
[38] P. Klaer, C.A. Jenkins, V. Alijani, J. Winterlik, B. Balke, C. Felser, H.J. Elmers, Appl. Phys. Lett. 98 (2011) 212510.
[39] V. Alijani, J. Winterlik, G.H. Fecher, C. Felser, Appl. Phys. Lett. 99 (2012) 222510.
[40] P. Hohenberg, W. Kohn, Phys. Rev. 136 (1964) B864.
[41] W. Kohn, L.J. Sham, Phys. Rev. 140 (1965) A1133.
[42] S. Cottenier, Density Functional Theory and the Family of (L)APW-methods: A Step-by-stem Introduction (Instituut voor Kern-en Stralingsfysica, K.U. Leuven, Belgium). freely available at ⟨http://www.wien2k.at/reg_users/textbooks⟩.
[43] E. Sjöstedt, L. Nordström, D.J. Singh, Solid State Commun. 114 (2000) 15.
[44] G.K.H. Madsen, P. Blaha, K. Schwarz, E. Sjöstedt, L. Nordström, Phys. Rev. B 64 (2001) 195134.

[45] P. Blaha, K. Schwarz, G. Madsen, D. Kvasnicka, J. Lutiz, Computer Code Wien2k, An Augmented Plane Wave+Local Orbital Program for Calculating Crystal Properties, Karlheinz Schwarz, Technische Universität Wien, Austria, 1999.
[46] J.P. Perdew, K. Burke, M. Ernzerhof, Phys. Rev. Lett. 77 (1996) 3865.
[47] [a] G. Kresse, J. Halfner, Phys. Rev. B 47 (1993) 558;
[b] G. Kresse, J. Furthmüller, Comput. Mater. Sci. 6 (1996) 15;
[c] G. Kresse, J. Furthmüller, Phys. Rev. B 54 (1996) 11169 (see website ⟨http://cms.mpi.univie.ac.at/vasp/⟩).
[48] [a] G. Kreese, D. Joubert, Phys. Rev. B 59 (1999) 1758;
[b] P.E. Blöchl, Ibid 50 (1994) 17953.
[49] A. Jakobsson, P. Mavropoulos, E. Sasioğlu, S. Blügel, M. Ležaić, B. Sanyal, I. Galankis, Phys. Rev. B 91 (2015) 174439.
[50] T. Block, M.J. Carey, B.A. Gurney, O. Jepson, Phys. Rev. B 70 (2004) 205114.
[51] I. Galankis, P.H. Dederichs, N. Papanikolaou, Phys. Rev. B. 66 (2002) 174429.
[52] I. Galankis, Phys. Rev. B 71 (2005) 012413.